# Circulations Associated with a Mature-to-Decaying Midlatitude Mesoscale Convective System. Part II: Upper-Level Features

RICHARD H. JOHNSON

*Department of Atmospheric Science, Colorado State University, Fort Collins, Colorado*

DIANA L. BARTELS

*Mesoscale Research Division, National Severe Storms Laboratory, Boulder, Colorado*

(Manuscript received 18 July 1991, in final form 24 October 1991)

ABSTRACT

The vertical structure of a midtropospheric mesovortex that developed during the decay of a midlatitude mesoscale convective system over Kansas and Oklahoma on 23–24 June 1985 is documented. Surface, rawinsonde, wind profiler, and dual-Doppler data are used to define its structure.

As has been observed in other midlatitude and tropical cases, the mesovortex occurred within the trailing stratiform precipitation region of a squall-line system. It was associated with a preexisting synoptic-scale shortwave trough, and as the circulation developed, it deformed the back edge of the stratiform precipitation region into a hooklike pattern. The ~100–200-km mesovortex was confined to the midtroposphere (3–8 km), with a maximum amplitude just above the 0°C level. The vortex axis sloped toward the northeast, but its orientation changed hour by hour over the 2-h period of dual-Doppler coverage. Overall, the mesovortex was warm core, although its thermal structure was complex and apparently significantly influenced at the analysis time by a descending rear-inflow jet entering the rear portion of the stratiform region. The warmest anomaly was found at low levels (near 850 mb) with a shallow cool anomaly in the midtroposphere near the 0°C level and a weak warm anomaly aloft. At 500 mb the warmest air was shifted to the north of the vortex center, where the atmosphere was also relatively dry, while at 400 mb (near the top of the mesovortex) the warmest air coincided with the vortex center.

Although the mesovortex was sampled for only a brief portion of its lifetime, the observations suggest a close coupling between synoptic, mesoscale, and even microscale (cloud) processes in its formation. A vorticity budget based on the sounding data *during the decaying stage of the storm* indicates that convergence production of vorticity associated with a mesoscale updraft–downdraft couplet in the stratiform precipitation region was a critical factor in intensifying the circulation at that time. Vorticity production by tilting played a minor role during this period due to relatively weak environmental wind shear. The weak shear, however, likely contributed to the longevity of the mesovortex.

## 1. Introduction

This paper is the second in a series aimed at documenting the structure of a midlatitude, mesoscale convective system over Kansas and Oklahoma that contained in its decaying stage a midtropospheric cyclonic circulation or *mesovortex*[1] (Zhang and Fritsch 1987, 1988a,b). The convective system occurred on 23–24 June 1985 during the Oklahoma–Kansas Preliminary Regional Experiment for STORM-Central (OK PRESTORM). In Part I (Johnson et al. 1989), we investigated surface features accompanying the storm's decay. Three significant phenomena were identified: 1) a pronounced wake low and associated intense surface pressure gradient at the back edge of the trailing stratiform precipitation region, 2) surface heat bursts (Johnson 1983) outside the precipitation area but in the vicinity of the wake low, and 3) a developing strong surface mesolow (distinct from the wake low) during a 2-h period of the final decay of the stratiform region. The existence of these features was found to be closely linked to strong downdrafts in the lower troposphere.

In this second paper we examine the vertical structure of the mesovortex that developed within the stratiform precipitation region using surface, sounding, wind profiler, and Doppler radar data. This circulation is of the type described by Johnston (1982), Bartels and Maddox (1991), and Zhang and Fritsch (1987, 1988a,b) that, following the dissipation of the cirrus cloud shield of a mesoscale convective system, takes

[1] These features have alternatively been referred to as *mesoscale vorticity centers* (MVCs) by Johnston (1982) and *midlevel cyclonic vortices* (MCVs) by Bartels and Maddox (1991).

*Corresponding author address:* Dr. Richard H. Johnson, Colorado State University, Department of Atmospheric Science, Fort Collins, CO 80523.

on a tropical cyclonelike appearance from a satellite perspective, that is, a spiral band structure consisting of primarily low-to-midlevel clouds. Cyclonic circulations associated with the stratiform regions of precipitation systems have been observed both in the tropics (Houze 1977; Leary 1979; Gamache and Houze 1982; Houze and Rappaport 1984) and at midlatitudes (e.g., Ogura and Liou 1980; Smull and Houze 1985; Leary and Rappaport 1987). They show up as a prominent feature of the decaying stage of an MCC (mesoscale convective complex; Maddox 1980, 1983) composite life cycle as determined by Cotton et al. (1989). These circulations appear to be so prevalent that they have now emerged as one of the primary organizational characteristics identified within one class of mesoscale convective systems over the central United States based on climatological studies of radar data (Houze et al. 1989, 1990). They have been commonly observed to last for days (Wetzel et al. 1983; Kuo et al. 1986; Zhang and Fritsch 1987, 1988b; Menard and Fritsch 1989) and during the daytime hours have been observed to couple with the boundary layer to generate subsequent deep convection, as occurred in our case (Part I).

In a recent study using conventional sounding data, Bartels and Maddox (1991) investigated the composite kinematic and thermodynamic characteristics of 24 mesovortices identified by visible satellite imagery over an 8-yr period over the central United States. They determined that these circulation features typically form in large-scale environments characterized by weak flow, weak vertical shear, and weak background relative vorticity. Convergence of planetary vorticity was found to be the dominant mechanism for the spinup of the midlevel circulations. The typical horizontal scale of the mesovortices, as determined by satellite, was between 150 and 300 km, substantially less than the average ~400-km-scale conventional rawinsonde station spacing.

Observations from OK PRE-STORM are of sufficient resolution to allow documentation of the detailed structure of mesovortices, even if only for brief portions of their lifetimes. Brandes (1990) studied a mesovortex that developed in proximity to the trailing stratiform region of a mesoscale convective system that occurred over Oklahoma on 6–7 May 1985. In that instance, a cyclonic circulation extended from near 1 to 8 km and had a cold core at low levels (below 5 km) and a warm core above. Dual-Doppler radar data indicate that the cyclonic flow deformed the stratiform region into a hooklike pattern. A mesovortex also occurred on 28 May 1985 over Kansas in association with a mesoscale convective system that had organizational characteristics similar to those on 6–7 May (Houze et al. 1989). The vortex had a similar depth and deformed the stratiform region in a similar way, but its thermal structure could not be determined due to an absence of sounding data. Biggerstaff and Houze (1991) studied the midlevel vorticity structure of the 10–11 June squall line, although in that case a long-lived mesovortex did not form. On a somewhat smaller scale, Verlinde and Cotton (1990) documented with dual-Doppler radar data a highly transient, mesovortex couplet having ~50-km horizontal dimension that occurred on 16–17 June 1985.

The causes of mesovortex formation are still a matter of some debate, although recent modeling results (Marroquin and Brown 1986, personal communication; Zhang and Fritsch 1987, 1988a,b) suggest that resolvable-scale (stratiform) latent heat release is the primary contributor to the circulation spinup. This result is expected for situations where the horizontal scale of the heating is comparable to or larger than the Rossby radius of deformation (Schubert et al. 1980; Zhang and Fritsch 1988a; Cotton et al. 1989), such that much of the energy from the heating goes into quasi-balanced flow. Smaller-scale, short-lived circulations [for example, those studied by Smull and Houze (1985), Stirling and Wakimoto (1989), and Verlinde and Cotton (1990)] have been referred to by Cotton et al. (1989) as "dynamically small" and are distinct from the type of mesovortex studied in this paper.

The concept of diabatic processes contributing to the development of mesovortices is consistent with the tropical mesoscale anvil modeling study of Brown (1979), wherein a prominent mesolow was found to develop at the base of the mesoscale anvil cloud due to condensation heating aloft and evaporative cooling at low levels. This mechanism is discussed in Zhang and Fritsch (1988a). It is also supported by the theoretical studies of Raymond and Jiang (1990) and Hertenstein and Schubert (1991) concerning potential vorticity anomalies associated with squall lines. Hertenstein and Schubert found that a heating profile resembling that associated with a squall line containing a trailing stratiform region (heating aloft and cooling in the lower troposphere) leads to a strong positive potential-vorticity anomaly in the midtroposphere. The associated cyclonic circulation that develops at midlevels can be interpreted as a quasi-balanced flow response to the heating. Since midlevel mesovortices are frequently long-lived features, this interpretation of their dynamics is an attractive one. However, the detailed evolution of the vorticity field in each instance may be rather complex (Biggerstaff and Houze 1991; Zhang 1992).

It is remarkable that while the number of studies of mesovortices has grown considerably in recent years, observations of the detailed kinematic and thermodynamic structure and vorticity dynamics of these systems remain sparse. Undoubtedly, this situation is a result of their relatively small horizontal scale. There is some suggestion that the circulations are warm core (e.g., Zhang and Fritsch 1987, 1988a,b), but observations of the temperature field within the vortices are notably lacking. The National Oceanic and Atmospheric Administration (NOAA) WP-3D research aircraft flights into a mesovortex occurring at approxi-

mately the same time, but nearly 800 km northeast of the system studied in this paper, indicated a warm area about 50 km north of the circulation center near 500 mb; however, there were insufficient data to document its vertical structure (Bartels 1989). In Part I, a warm core was also reported at 500 mb in the western system over Kansas, but the warm center was again apparently shifted somewhat north of the circulation center. Knowledge of the thermal structure of mesovortices is relevant to understanding their dynamics as well as to answering the question of whether such systems in the tropics may serve as incipient disturbances for tropical cyclones, as has been suggested by Velasco and Fritsch (1987). In any event, further information on the vertical structure of mesovortices is sorely needed, and it is the primary purpose of this paper to add to our knowledge of this aspect of such systems.

## 2. Data analysis and procedures

### *a. Soundings*

A discussion of the surface- and upper-air networks employed in OK PRE-STORM is given in Part I. Unfortunately, releases from the special rawinsonde network were not initiated until 0430 (all times UTC), a time somewhat after the formation of the mesovortex. Special releases then continued for only two additional times, 0600 and 0900, and even then only for a subset of the entire network of sounding stations. In the use of the rawinsonde data, account is taken for both balloon drift and variable release times. Data from the 50-MHz wind profiler at Liberal, Kansas, have also been incorporated into the analyses.

### *b. Surface data*

Treatment of the 5-min surface pressure data from the National Center for Atmospheric Research (NCAR) Portable Automated Mesonetwork (PAM II) and National Severe Storms Laboratory (NSSL) Surface Automated Mesonetwork (SAM) stations is the same as in Part I. Pressures have been adjusted hydrostatically to 518 m, and atmospheric tidal effects have been removed.

### *c. Doppler radar data*

To probe the internal precipitation and kinematic structure of the storm, dual-Doppler analyses were performed using data from the NCAR CP-3 and CP-4 C-band radars. Coordinated scans initiated at 0530, 0637, and 0720 were chosen for analyses as the storm's trailing stratiform precipitation region passed through the southwest lobe of the dual-Doppler domain. A single-Doppler analysis from the CP-3 radar volume scan initiated at 0423 (not presented here) provided additional continuity of the reflectivity structure; however, a dual-Doppler analysis at this time was not possible since the stratiform precipitation region was outside the range of CP-4.

Details of the radars and their scanning strategies are provided by Rutledge et al. (1988). For this case, both radars were operated in coordinated sector scans designed to sample the stratiform precipitation region of the western system. Most scans stepped through 21 elevation angles from 0.3° to 22° and required at most 5 min to complete. The 0720 scan, however, was a full 360° scan through 14 elevation angles and required 6.25 min to complete.

For each analysis, single-Doppler measurements were first edited interactively to identify and correct velocity and range aliasing and eliminate other sources of contamination. These data were then interpolated to 90-km × 90-km × 14-km rectangular grids with a spacing of 1 km in all coordinate directions, with the lowest analysis level at 0.5 km AGL.[2] Translation of features during the finite scanning interval was taken into account, and the analysis times of 0532, 0639, and 0723 represent the approximate midpoints of the scanning intervals. Synthesized horizontal winds ($u$, $v$) following Ray et al. (1980) and the maximum reflectivity measured by either radar were computed at each grid point. These values were then subjected to a Shuman filter such that small convective-scale features of wavelengths < 10 km were strongly damped. Vertical air motion ($w$) was then calculated using downward integration of the anelastic continuity equation subject to the condition of vanishing $w$ at upper and lower boundaries.

All horizontal winds derived from the Doppler radar data are viewed in a frame of reference attached to the stratiform precipitation region as it passed over the Kansas Doppler network. The motion of the stratiform region (toward 170° at 5 m $s^{-1}$) was determined by tracking successive low-level PPI scans during the Doppler analysis period (0430–0730) from the WSR-57 radar located at Wichita, Kansas. However, the leading line of convection exhibited a storm motion toward 170° at 10 m $s^{-1}$ and is the reference frame used to view the larger-scale sounding, surface, and wind profiler data. Brandes (1990) also found that the mesovortex (and associated stratiform precipitation region) moved at less than half the speed of the leading convective line.

The locations of CP-3, CP-4, Wichita, and the 90-km × 90-km 0532 dual-Doppler analysis domain are shown in Fig. 1. The analysis domain used at 0639 and 0723 was shifted 12 km to the south of that at 0532 to account for the motion of the stratiform precipitation region to the south.

## 3. Synoptic setting

The reader is referred to Part I for a more thorough discussion of the background synoptic conditions for this case. The storm under investigation developed

[2] All Doppler data are referred to AGL (above ground level), which in the area of study is ~0.5 km above sea level.

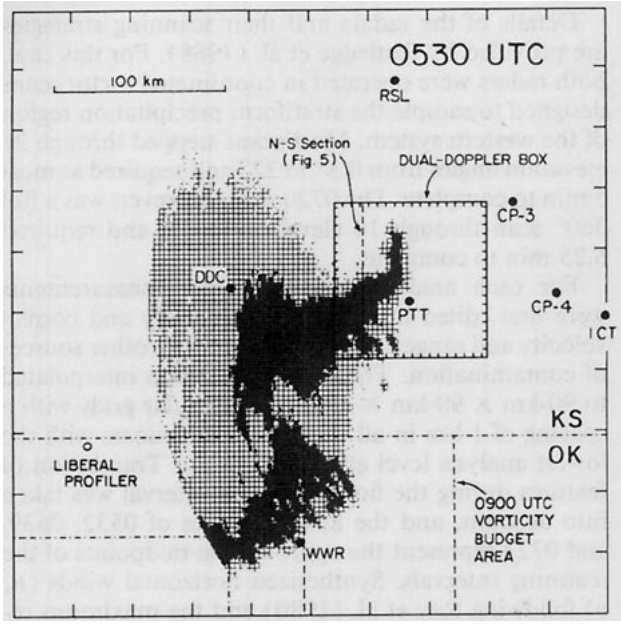


FIG. 1. Radar reflectivity field from Wichita, Kansas, (ICT) WSR-57 radar at 0530 UTC and 90-km × 90-km dual-Doppler analysis box from CP-3 and CP-4 radars. Also indicated are position of a north–south cross section in Fig. 5, 0900 UTC vorticity-budget area, and sounding sites. Reflectivity thresholds are 25, 44, and 49 dBZ.

within a 500-mb ridge over the central United States and had an environment characterized by weak winds and weak vertical wind shear. It was the westernmost of two mesoscale convective systems that traversed the Midwest on the afternoon and evening of 23 June, as depicted by infrared satellite imagery at 0430 in Fig. 2a. The eastern system was investigated by NOAA WP-3D research aircraft. It was the western system, however, that tracked through the OK PRE-STORM network. Both storms were characterized in their mature stages by arc-shaped leading convective lines on their southern peripheries and trailing stratiform regions to the north. It was reported in Part I that the mesovortex formation appeared to occur at midlevels during the mature stage of the storm with an amplification of the circulation over northwestern Oklahoma as the stratiform precipitation region decayed (see satellite picture at 1001 in Fig. 2b). There is only a slight hint of a vortex at this time. In fact, satellite evidence of a mesovortex was so weak for this case that the system was not among those included in the survey study of Bartels and Maddox (1991). Nevertheless, it did produce a pronounced mesovortex.[3] On the day following the mesovortex spinup, new deep convection broke out in the vicinity of the remnant circulation.

[3] Bartels and Maddox (1991) note that it is not uncommon for a mesovortex to occur in the absence of a prominent signature in the satellite imagery.

## 4. Mature stage of stratiform region

### *a. Broad-scale structure*

The low-level reflectivity pattern in the western storm is illustrated in Fig. 3a. The primary features were a leading convective line and a distinct, broad trailing stratiform precipitation region. The isolated area of enhanced stratiform rainfall in Fig. 3a had existed for the previous ~3 h (Fig. 9, Part I). The 518-m pressure analysis at 0530 shows a pronounced mesohigh centered between the convective line and the enhanced trailing stratiform region with vigorous outflow over a large area, indicating strong, lower-tropospheric subsidence on the mesoscale. A rather deep wake low existed to the rear (on the north side) of the stratiform region with an enhanced lobe of low pressure inside the cusp in the reflectivity field (5-min surface data have been used in the construction of the surface pressure analysis in Fig. 3a). To the south of this area a very strong pressure gradient existed, locally up to 1 mb $km^{-1}$ [estimated from a time-to-space conversion of the pressure trace at PAM station 19 (P19), where a fall of 4 mb in 15 min was observed]. During the rapid pressure fall at P19, stratiform rain fell at a rate of 3–5 mm $h^{-1}$ (ending at 0530, the time of lowest

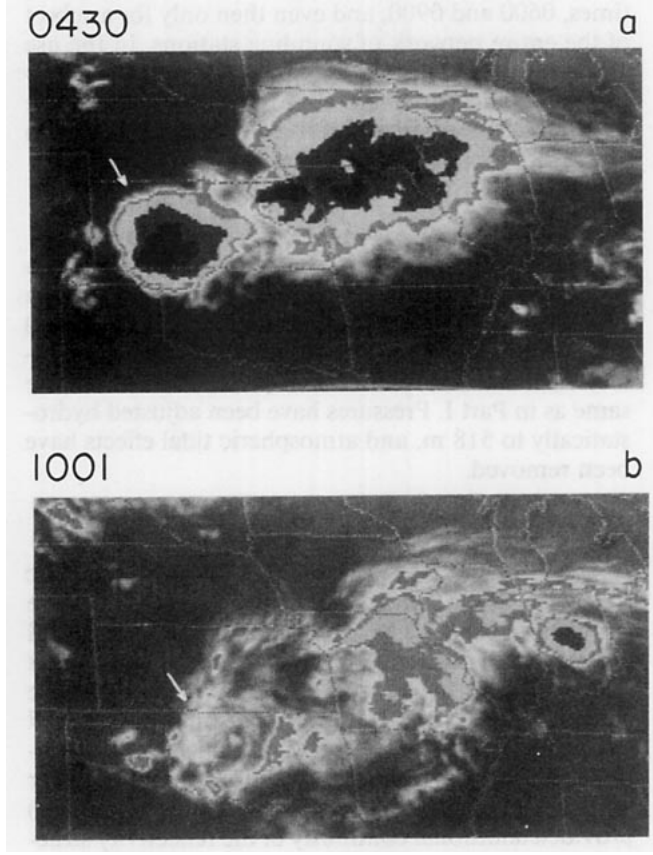


FIG. 2. Infrared satellite pictures at (a) 0430 and (b) 1001 UTC 24 June 1985. Arrows indicate system under investigation.

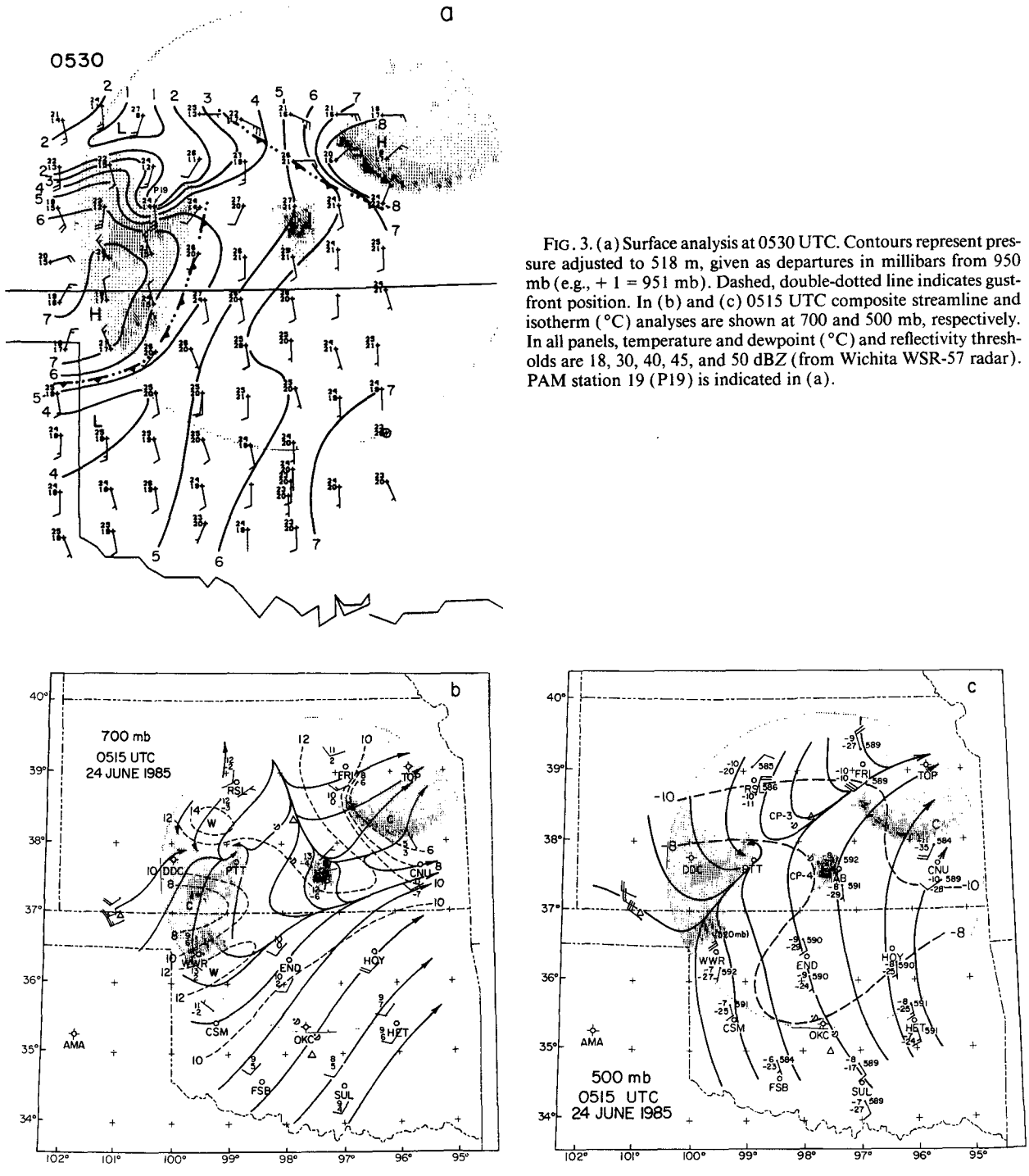


FIG. 3. (a) Surface analysis at 0530 UTC. Contours represent pressure adjusted to 518 m, given as departures in millibars from 950 mb (e.g., + 1 = 951 mb). Dashed, double-dotted line indicates gust-front position. In (b) and (c) 0515 UTC composite streamline and isotherm (°C) analyses are shown at 700 and 500 mb, respectively. In all panels, temperature and dewpoint (°C) and reflectivity thresholds are 18, 30, 40, 45, and 50 dBZ (from Wichita WSR-57 radar). PAM station 19 (P19) is indicated in (a).

pressure), the wind shifted from westerly at 6 m $s^{-1}$ to southerly at 15 m $s^{-1}$, the temperature jumped from 21° to 25°C, and the relative humidity dropped from 70% to 50%. The surface temperature and moisture changes at P19 resemble those accompanying the heat bursts at PAM stations 2, 3, 4, 10, 11, and 12 (Part I), but they are not quite as dramatic.

Intense pressure gradients between mesohighs and wake lows have also been observed in several other PRE-STORM cases: 6–7 May (Brandes 1990); 28 May (Rutledge, personal communication); 3–4 June (Stumpf et al. 1991), and to a lesser extent, 10–11 June. This phenomenon has been shown by Johnson and Hamilton (1988), Stumpf et al. (1991), and Smull et al. (1991) to be a surface manifestation of strong lower-tropospheric subsidence within the rear-inflow

jet at the trailing edge of the stratiform rainfall. A similar finding for this study will be confirmed momentarily. There is no evidence of an extension of the mesovortex (at least as a closed circulation) to the surface, consistent with the findings of Zhang and Fritsch (1988b) and Brandes (1990) for the cases they studied.

The flow at 700 mb at 0515 is presented in Fig. 3b. In order to enhance the data coverage, soundings at 0430 and 0600 have been formed into a composite, assuming a storm motion toward 170° at 10 m $s^{-1}$. Data for streamline analyses in the precipitation areas are sparse, except in the region of the dual-Doppler analyses (near PTT). In this location dual-Doppler–derived winds have been incorporated into the streamline analysis. Doppler-derived winds (shown in more detail later) indicate a cyclonic circulation on the northern periphery of the stratiform region with the curved flow conforming to a cusp in the reflectivity field there. The converging airstreams at the rear of the stratiform region fed strong downdrafts in the lower troposphere (subsection 4b).

Several axes of diffluence are seen at 700 mb outside the convective areas (Fig. 3b), both ahead of the convective line and between the two mesoscale convective systems. The divergence ahead of the convective line is probably associated with presquall compensating subsidence, as described by Hoxit et al. (1976) and Fritsch and Chappell (1980). Similar flow at this level and in this location was reported for the 10–11 June 1985 squall line by Johnson and Hamilton (1988). The northwest–southeast diffluence axis centered between the two mesoscale convective systems is likely a manifestation of midtropospheric subsidence between the two storms, a phenomenon that Stensrud and Maddox (1988) argued suppressed new development of convection along the storms' low-level converging outflows.

At 500 mb (Fig. 3c), an elongated northeast–southwest trough axis extended across the stratiform regions of the two storms. This trough is part of a synoptic-scale minor short-wave disturbance that was progressing through a large-scale ridge over the central United States (Fig. 3, Part I). Zhang and Fritsch (1987, 1988a,b) also found a short-wave trough in association with the mesovortex developments they studied, but it is not clear whether or not such troughs are always necessary for mesovortex development. Finally, at 200-mb pronounced anticyclonic flow occurred above and in advance of the two convective systems (not shown).

### *b. Finescale structure*

We next shift the attention to a dual-Doppler analysis at 0532 over a 90-km × 90-km box encompassing the mesovortex center near the eastern portion of the cusp at the northern edge of the stratiform region (Fig. 1). The system-relative flow within the mesovortex at 0532 at various levels in the troposphere is illustrated in Fig. 4. At low levels (2.5 km AGL, Fig. 4a), generally southerly, cyclonically curved flow occurred through the north–south-oriented stratiform precipitation appendage. Maximum reflectivities reached 30–40 dBZ along and to the north of the precipitation axis with the strongest reflectivity gradients on the northern periphery of the region.

Moving up to 4.5 km AGL, a greater fraction of the analysis area was filled with precipitation (Fig. 4b). At this level a closed cyclonic circulation was present, centered just west of the north–south precipitation arm. From the analysis at this level (both at 0532 and in a single-Doppler analysis conducted at 0423), there is the strong suggestion that the mesovortex itself was creating the hooklike reflectivity pattern (as in Brandes 1990) by carrying hydrometeors northward on its east side and eroding them on the west, perhaps through the effects of sublimation and evaporation. A closed circulation was also present in the actual winds (not shown). Although the northerly winds that complete the circulation at 4.5 km cannot be seen at 2.5 km (nor at 3.5 km) due to the lack of scatterers, the surrounding sounding data (e.g., as seen at 700 mb or 2.5 km AGL in Fig. 3b) suggest that a closed circulation may have existed down to these levels. Liberal, Kansas, wind profiler data, taken at a later stage in the life of the system (section 5), indicate that the lowest extension of the circulation was to about 3.0 km AGL.

At 6.5 km (Fig. 4c) a pronounced mesovortex was still evident, along with a slight deformation of the reflectivity field by the cyclonic flow. The circulation was still present, although much weaker, at 8.5 km (Fig. 4d). Above this level the mesovortex disappeared, and by 10 km the flow became generally anticyclonic and divergent over the entire system.

A north–south cross section of reflectivity and system-relative winds at a position just west of the mesovortex center (74 km to the west of CP-3; position indicated in Fig. 1) is shown in Fig. 5. The strong reflectivity gradient at low levels in this figure marks the northern boundary of surface rainfall as well as a pronounced zone of midtropospheric convergence of front-to-rear flow from the south and rear-to-front flow (or a rear-inflow jet; Smull and Houze 1987) from the north. This converging flow descended (with speeds up to 6 m $s^{-1}$) in a narrow ~10-km zone. Collocated with this zone of strong descent was a band of intense surface pressure gradients (Fig. 3a). The system-relative flow and reflectivity pattern in the cross section (Fig. 5), as well as the coincident intense surface pressure gradient, show a remarkable resemblance to those observed at the rear edge of a trailing stratiform precipitation region that occurred over Kansas on 3–4 June 1985 (Stumpf et al. 1991). It was argued in Stumpf et al. (1991) and verified by Smull et al. (1991) using the dual-Doppler dynamic retrieval technique that the strong descent in a region of a sharp reflectivity gradient led to a strong gradient in subsidence warming at low levels, thereby creating hydrostatically a rapid local variation in the surface pressure. The vertical cross sec-

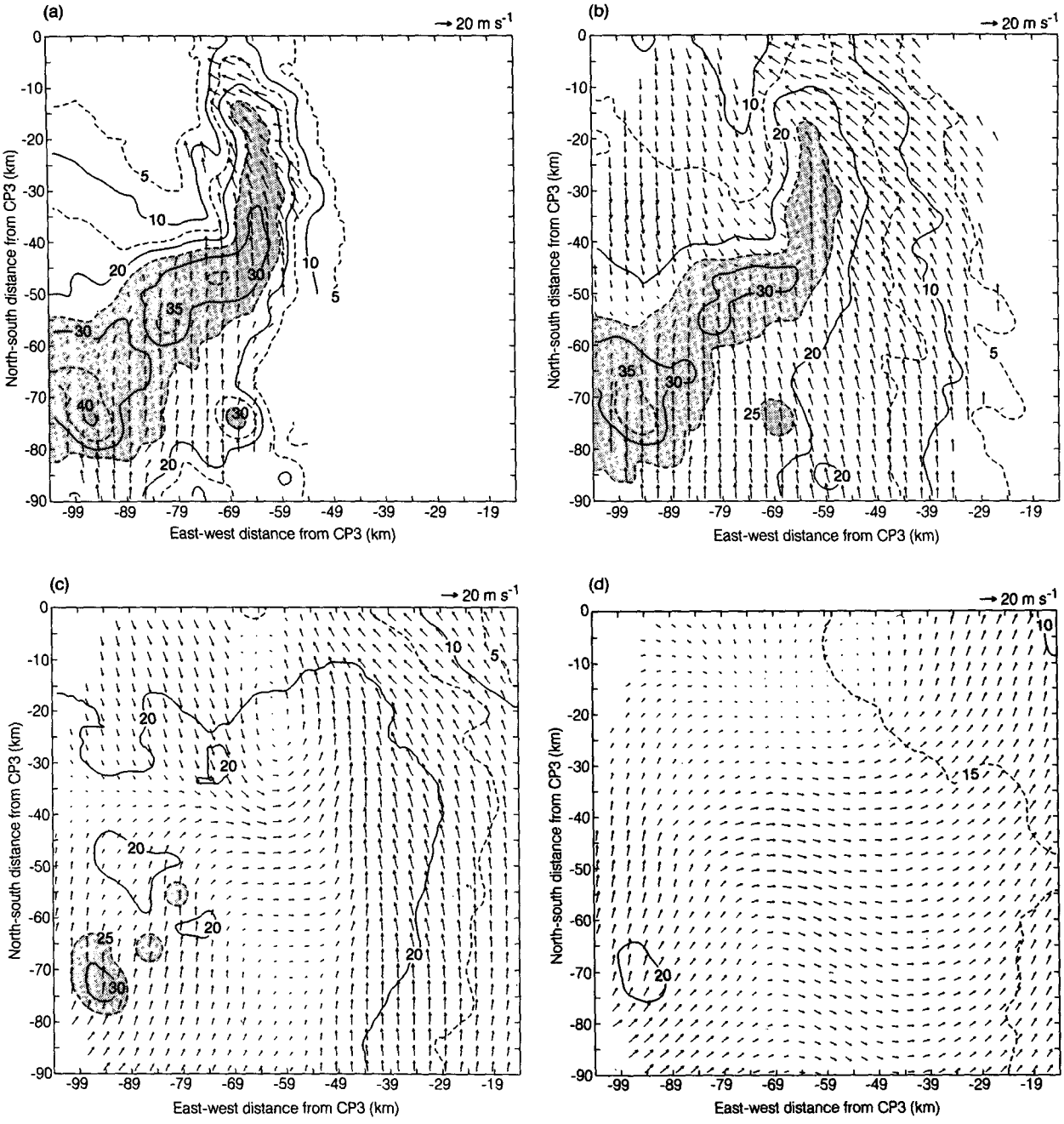


FIG. 4. Reflectivity (contours, 5-dBZ interval starting at 5 dBZ, stippling for values > 25 dBZ) and system-relative winds (m $s^{-1}$, scale at upper right, plotted at every third grid point) at (a) 2.5 km, (b) 4.5 km, (c) 6.5 km, and (d) 8.5 km at 0532 UTC.

tion in Fig. 5 across the zone of intense surface pressure gradient (Figs. 1 and 3a) presents yet another example of this process and points to, along with the heat bursts documented in Part I, important surface dynamical consequences of stratiform precipitation regions to the rear of squall lines.

The sounding and Doppler observations at this mature stage of the stratiform region have been merged into a general depiction of the overall airflow and thermodynamic properties of the system in Fig. 6 [see Fig. 1 for locations of Doppler section and RSL (Russell, Kansas), PTT (Pratt, Kansas), and WWR (Woodward, Oklahoma)]. Doppler radar data over an 84-km north–south distance 74 km west of CP-3 have been placed onto a north–south vertical cross section of sounding data taken between 0430 and 0600 (Fig. 6a). Time-to-space conversion of the sounding data in Fig. 6 is based on a 10 m $s^{-1}$ southward motion of the system. The primary components of the circulation are: a front-to-rear flow through the leading convective line

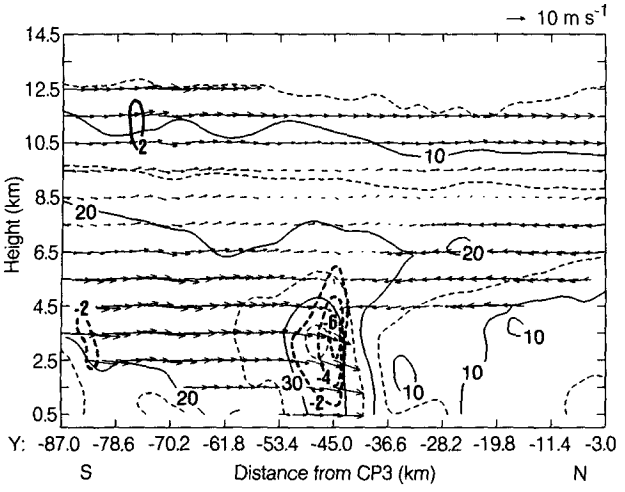


FIG. 5. North–south vertical cross section of system-relative winds (m s$^{-1}$, scale at upper right), radar reflectivity (5-dBZ interval starting at 5 dBZ) and vertical velocities (>2 m s$^{-1}$ heavy solid, < −2 m s$^{-1}$ heavy dashed, 2 m s$^{-1}$ intervals) at a distance 74 km west of CP-3 at 0532 UTC. See Fig. 1 for position of section.

and into the trailing stratiform region, a rear-to-front flow aloft ahead of the storm, a rear-to-front flow at midlevels at the rear of the storm (the rear inflow jet) descending into a front-to-rear flow at low levels out the back, and an overturning circulation or rotor just behind the convective line. This flow pattern bears a close resemblance to that determined for GATE [Global Atmospheric Research Program (GARP) Atlantic Tropical Experiment] squall lines (Houze 1977; Zipser 1977; Gamache and Houze 1982), West African squall lines (Roux et al. 1984), and other midlatitude squall lines (Ogura and Liou 1980; Smull and Houze 1985; Johnson and Hamilton 1988; Houze et al. 1989). However, in this instance there did not appear to be a penetration of the rear-inflow jet through the stratiform region toward the convective line (Fig. 5). The rear inflow appeared to be "blocked" by the stratiform precipitation region, as also occurred in the 3–4 June case studied by Stumpf et al. (1991). The moderate stratiform precipitation associated with this blocking also appears to be critical in driving the low-level rear-to-front flow at the base of the rotor in this case. These findings are consistent with and support the mechanism proposed by Lafore and Moncrieff (1989) for the generation of vorticity within the squall-line rotor through evaporatively driven subsidence within the stratiform region.

A north–south cross section of the equivalent potential temperature $\theta_e$, temperature anomaly, and relative humidity fields across the storm is presented in Fig. 6b. The temperature anomalies represent departures from the mean temperature ahead of the squall line determined by subjective analyses of rawinsonde data composites at 0515 (e.g., as shown in Fig. 3) at 100-mb intervals. Surface mesonetwork data have been used to determine the surface anomalies. Warm anomalies in the leading convective line updraft may be underestimated. The primary features are 1) a warm, dry region in the midtroposphere over a 100-km distance ahead of the line (associated with the presquall mesolow, Hoxit et al. 1976), 2) a pronounced cold anomaly near the surface within the stratiform rain region (associated with the surface mesohigh, e.g., Fujita 1955), and 3) a strong warm, dry anomaly centered near 850 mb at the rear edge of the trailing stratiform region (associated with the wake low; e.g., Johnson and Hamilton 1988). A midtropospheric $\theta_e$ minimum existed ahead of the squall line but was absent to the rear as low-$\theta_e$ air extended all the way to the surface. The warm anomaly at upper levels in the stratiform region cannot be substantiated with sounding data at this time (note sounding positions, large dots, in Fig. 6a) but is confirmed by sounding data at 0900 (subsection 6b).

## 5. Decaying stage of stratiform region

As described in Part I, the stratiform precipitation region decayed rapidly over the next 3-h period (0600–0900). By 0900 all of the rainfall had ceased. The latest time at which reliable dual-Doppler analyses of the mesovortex could be obtained was 0723, so surface analyses near this time will be presented (surface analyses at 1-h intervals from 0600 to 1200 are shown in Part I). A dual-Doppler synthesis was also completed at 0639, but the results from it are essentially intermediate to the 0532 and 0723 volumes and, therefore, are not presented. Although a few soundings were released at 0600, the best coverage was at 0900. Therefore, upper-air analyses at 0900 will be shown.

The low-level Wichita radar reflectivity field and 518-m pressure field at 0725 are displayed in Fig. 7a. By this time the leading convective line had dissipated. A stratiform precipitation region remained with a lobe of high pressure beneath it. A wake low was still present to the north with a strong, although somewhat reduced, pressure gradient along the northern boundary of the stratiform region. However, the cusp in the radar reflectivity field that was present at 0530 (Fig. 3a) vanished by 0725, as had the small-scale low pressure area within it (Fig. 7a).

At 500 mb the closed circulation that was observed earlier at 0515 on a small scale within the southwest–northeast trough over the region (Fig. 3c) expanded and was beginning to separate from the second closed circulation to the northeast (Fig. 7b). A preliminary version of this analysis was presented in Zhang and Fritsch (1987) and Part I, but the figure has now been modified based on dual-Doppler analyses to show a closed circulation associated with the western system. A warm core is also indicated at 500 mb; however, as noted in Part I, its center appears to have been displaced to the north of the trough axis. Here again, the precise

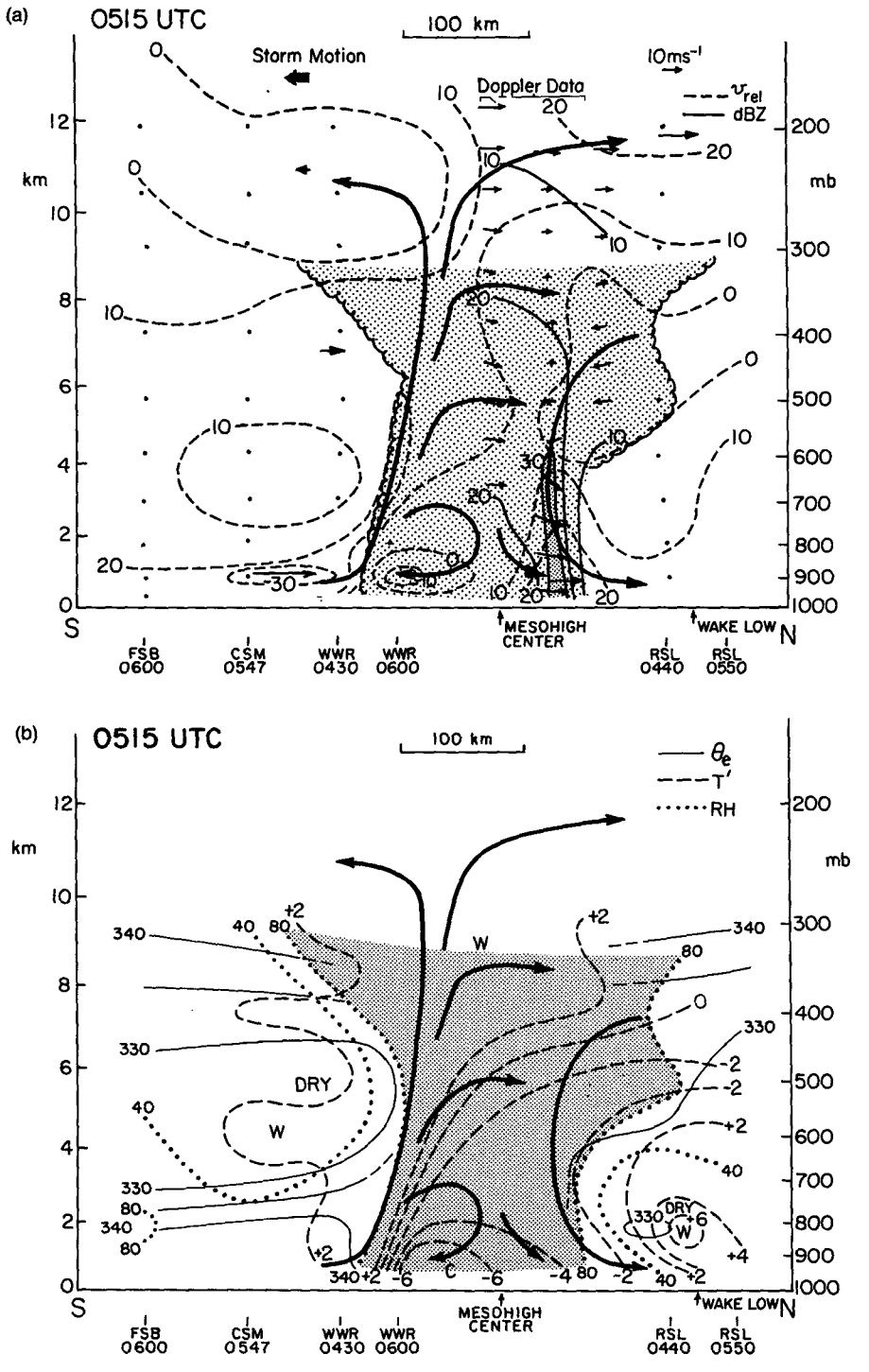


FIG. 6. (a) Composite north–south vertical cross section at 0515 UTC of storm-relative $v$ component of the flow (m s$^{-1}$, dashed), using a southward storm motion of 10 m s$^{-1}$, including dual-Doppler segment of winds and reflectivity (dBZ, solid; >30 dBZ dark shading). Light-shaded interior of scalloped curve denotes RH > 80% (with respect to ice at temperatures below freezing). Heavy arrows indicate storm-relative flow. Large dots indicate sounding positions. (b) Equivalent potential temperature (K, solid), temperature anomaly (K, dashed; departures from presquall average sounding), and relative humidity (%, dotted; values > 80% shaded). Contours of $\theta_e$ are terminated within the storm.

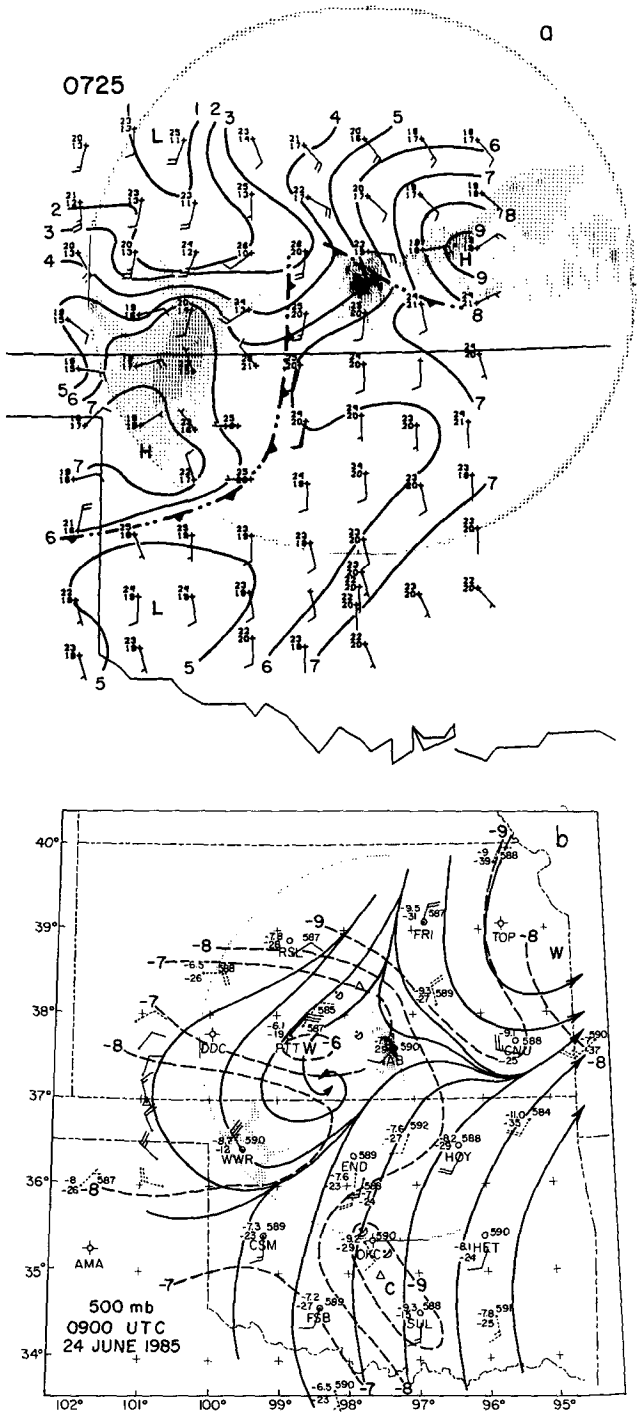


FIG. 7. As in Fig. 3, except at 0725 UTC in (a) and at 0900 UTC in (b). In (b) data 3 h earlier and later than 0900 UTC are indicated by dashed wind barbs.

position of the warm core cannot be accurately determined from the available data; however, the pattern depicted in Fig. 7b is similar to that measured directly by research aircraft within the mesovortex over Missouri (Bartels 1989).

As shown in Fig. 4 of Part I, the midlevel mesovortex drifted to the south into northwest Oklahoma by 1200. The development and movement of the mesovortex is well documented by a time series of ground-relative winds from the Liberal wind profiler (Fig. 8). The first evidence of the impact of the circulation at Liberal is within the 5–6.5 km MSL[4] (450–550-mb) layer around 0700 or 0730. The vortex then expanded vertically at Liberal, reaching a maximum depth there around 1200–1400, extending from 3.5 to 7 km (700–400 mb), and then appeared to have weakened after this time. The confinement of the mesovortex to the midtroposphere is dramatically illustrated in this wind profiler time series and may point to a unique ability of the planned National Weather Service wind-profiling network in capturing these phenomena. Since nonsteadiness of the mesovortex (in addition to propagation) may be significant over the long time period examined at Liberal, it must be cautioned that the wind time series cannot be used to unambiguously infer the character of the circulation development. Additionally, the horizontal scale of the mesovortex suggested by Fig. 8, assuming a constant speed of motion, is much greater than the 100–200-km scale determined by Doppler data. This discrepancy can be explained by an apparent slowing in the southward movement of the mesovortex motion after 0900.

The disappearance of the sharp curvature or cusp along the northern boundary of the stratiform region from 0530 to 0725, evident from a comparison of WSR-57 data in Figs. 3a and 7a, can also be seen in a comparison of the dual-Doppler analysis at 2.5 km AGL at 0723 (Fig. 9a) with that at 0532 (Fig. 4a). Southerly flow (all winds storm relative) throughout most of the stratiform region was still observed at 0723; however, much of the precipitation in the north–south appendage that existed at 0532 (Fig. 4a) had dissipated. A weakening of the cusp in the stratiform precipitation was also evident at 4.5 km (Fig. 9b), and a closed circulation, while inferred, was not completely defined by the data. Erosion of the echo on the north side of the circulation center was further evident at 6.5 km (Fig. 9c). Finally, at 8.5 km (Fig. 9d) the mesovortex was barely discernible. At all levels, the Doppler analysis at 0723 indicates a marked weakening of the precipitation intensity near the mesovortex center over the 2-h analysis period. This behavior is consistent with the observation of a near-complete demise of the stratiform region by 0900.

## 6. Vertical structure of mesovortex

### a. *Kinematic features*

The dissipation of the stratiform region is further illustrated in vertical profiles of radar reflectivity (Fig.

[4] Subtract 0.5 km to get elevation above ground level. Recall that all Doppler data are referred to AGL.

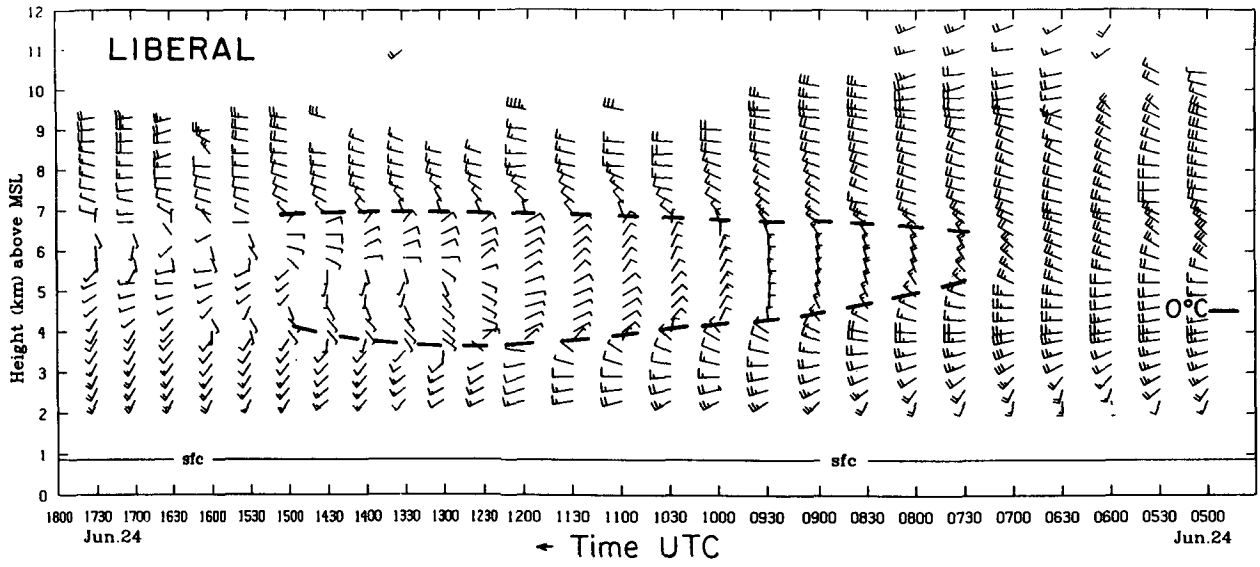


FIG. 8. Time series of Liberal, Kansas, profiler ground-relative winds from 0500 to 1730 UTC 24 June 1985. Dashed lines denote vertical extent of mesovortex.

10). Values in this figure represent averages over the precipitation-containing portion of the 90-km × 90-km analysis boxes. Because the precipitation volumes were only partially filled below 4 km, the structure of the curves at low levels must be interpreted with caution. The weakening of the stratiform region from 0532 to 0723 can be clearly seen; however, evidence of a brightband melting-layer structure (Leary and Houze 1979), while present at 0723, is missing at the other times due to incomplete volume filling. The average vertical velocity profile shows progressively weakening upward motion in the stratiform cloud aloft with time but increasing sinking motion below, reaching nearly 1 m $s^{-1}$ from 3 to 4 km at 0723.

The profile of $w$ in Fig. 10 indicates strong midlevel convergence. This convergence, which peaked near the 0°C level and increased in strength from 0532 to 0723, is illustrated in Fig. 11. Also shown in Fig. 11 is the domain-averaged relative vorticity, which also had a maximum in the midtroposphere. There is a vertical displacement between the peaks in convergence and relative vorticity, particularly at the later times 0639 and 0723. This feature may not be real but rather an artifact of partial filling of the analysis volume by precipitation. This effect can be seen by examining the horizontal pattern of divergence and vorticity in the mesovortex (Fig. 12). A displacement of the region of maximum vorticity is seen to the north of the region of maximum convergence, that is, to an area that in the later stages was not sampled by the radar as the storm dissipated (e.g., Figs. 9a,b). This weakening of the northern part of the circulation may, in part, explain the minima in echo-averaged relative vorticity near the 0°C level at 0639 and 0723 (Fig. 11). At best, it can probably be said that midtropospheric maxima in convergence and relative vorticity existed, strongly suggesting an important contribution by convergence to vorticity production in the mesovortex at this stage of its life cycle. This conclusion is supported by later computations of terms in the vorticity equation using rawinsonde data (section 7).

While peak values of divergence and relative vorticity averaged over a 90-km × 90-km box were 2–4 × $10^{-4}$ $s^{-1}$, they were locally an order of magnitude larger on the 2-km Doppler grid scale (Fig. 12). At 0532 a zone of strong convergence ($|\nabla \cdot \mathbf{v}| > 2 \times 10^{-3}$ $s^{-1}$) was located at 4.5 km along the interface between the front-to-rear flow and the rear-inflow jet, spiraling cyclonically in a broken fashion toward the vortex center (Fig. 12a). It is interesting to note that the magnitude of the divergence over most of the domain was rather weak, with large values concentrated in small areas, reminiscent of the process of scale contraction as a result of flow deformation (Welander 1955). The largest values of relative vorticity (locally exceeding 5 × $10^{-3}$ $s^{-1}$) were generally confined to a small region east and north of the vortex center (Fig. 12b). The positioning of the greatest values of vorticity in a region of strong convergence also suggests that the process of vortex stretching was operative.

### *b. Vertical tilt of mesovortex axis*

Careful inspection of Figs. 4 and 9 indicates that the center of the mesovortex sloped toward the northeast with height. This behavior is illustrated in Fig. 13, where the center position (at levels where it can be detected between 4.5 and 8.5 km) is plotted at 0532, 0639, and 0723 (all positions relative to CP-3). Based on the 6.5-km position, the mesovortex translated to the southeast

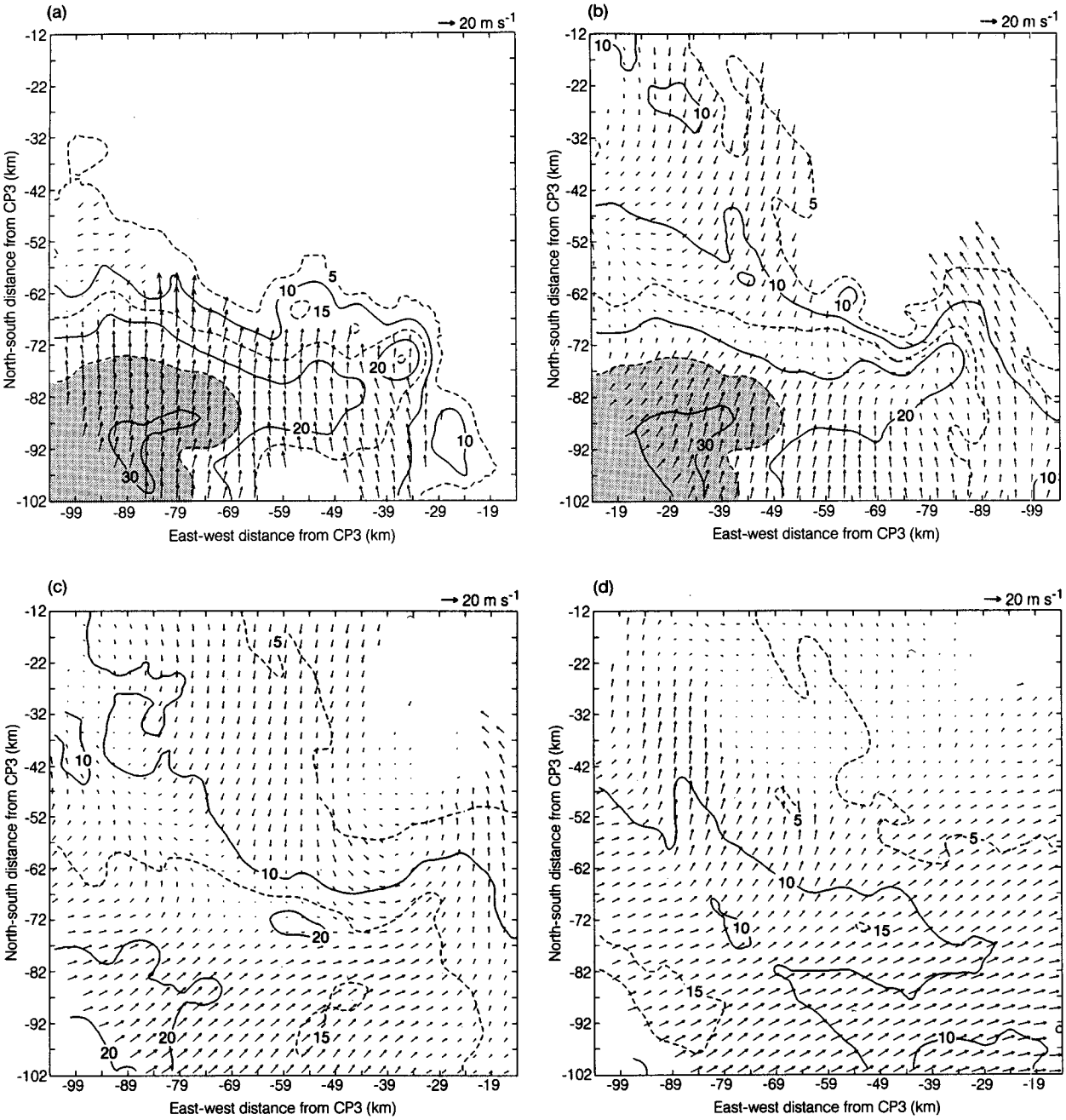


FIG. 9. As in Fig. 4, except at 0723 UTC.

at an average speed of 6 m $s^{-1}$. The tilt of the mesovortex was somewhat variable between 0532 and 0723, although its orientation remained toward the northeast throughout the period. The slope steadily decreased from 1:2.5 to 1:10 (the axis tilted away from vertical) during the 2-h time interval.

A northward component to the tilt of the mesovortex is further illustrated in computations of relative vorticity based on sounding data at 0900 (Fig. 14a; section along same north–south axis as in Fig. 6). The area of relative humidity > 80% (shading) is used to crudely depict the region of the dissipating stratiform cloud since by this time the system was out of the range of the research radars, and surface precipitation had ceased. The axis of maximum vorticity tilted toward the north with a 1:50 slope, although this value may be an underestimate due to sounding resolution limitations. Consistent with the dual-Doppler results at 0723 (Fig. 11), convergence and vorticity maxima were observed in the midtroposphere at the forward edge

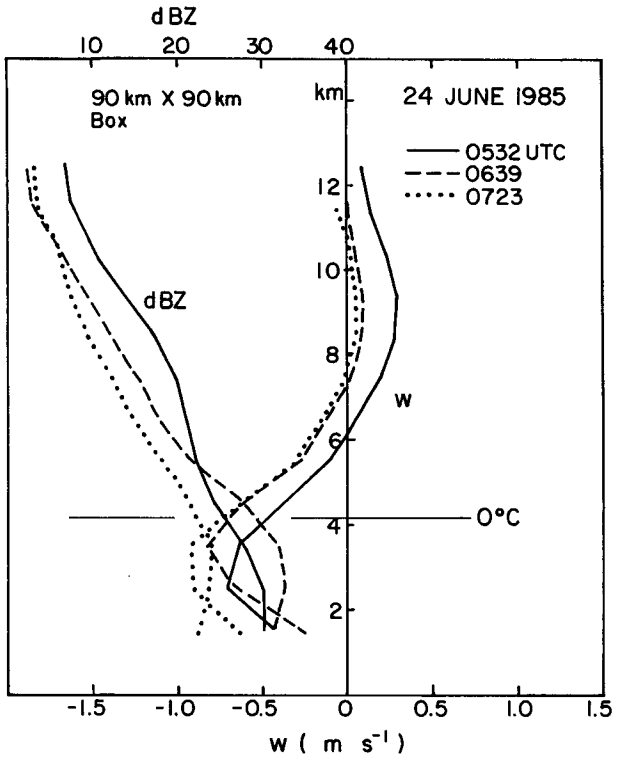


FIG. 10. Vertical profiles of radar reflectivity (dBZ) and vertical velocity (cm $s^{-1}$) averaged over the dual-Doppler domain at 0532, 0639, and 0723 UTC.

and near the base of the dissipating stratiform cloud, with divergence and negative vorticity aloft. A shallow layer of divergence near the surface existed beneath these maxima. These results show a strong resemblance to those obtained by Zhang and Fritsch (1988) in a numerical simulation of a mesovortex that occurred on 7–8 July 1982. Zhang and Fritsch also found a tilt of the mesovortex, with a slope intermediate to that given by the Doppler data at 0723 (Fig. 13) and that by the sounding data at 0900 (Fig. 14a). They attribute the tilt of the system (to the east in their case) to differential advection associated with the stronger westerlies aloft, a situation similar to that reported here (Fig. 3).

In Fig. 14b the vertical motion and system-relative north–south flow at 0900 are shown. A mesoscale updraft was observed within the leading edge of the dissipating stratiform cloud layer aloft. A mesoscale downdraft existed below along with a rear-inflow jet entering the system at midlevels, apparently feeding into the mesoscale downdraft. Consistent with the independently derived Doppler results (Fig. 10), the downdraft at this time was much stronger than the updraft, and the crossover between upward and downward motion was between 6 and 8 km. A region of rising motion at low levels was also detected to the north of the system. The latter feature was perhaps an indication of the beginning of a recovery of the system or a mesoscale oscillation (after Crook et al. 1990), whereby the low-level warm anomaly set up by the storm (temperature anomaly and moisture field are shown in Fig. 14c) later began to rebound (ascend due to buoyancy) and moisten the atmosphere. In Part I it was reported that 6 h later (at 1500), new boundary-layer–rooted deep convection broke out in the area to the north of the remnant vortex, perhaps as a consequence of this mesoscale oscillation.

While it can be argued from Fig. 14c that in an overall sense the mesovortex at 0900 was warm core, its thermodynamic structure was anything but simple. The strongest warm anomaly existed at low levels, centered near 850 mb, consistent with the modeling results of Zhang and Fritsch (1987, 1988a,b). A weaker warm anomaly existed in the decaying stratiform region aloft as well as far to the rear within a portion of the descending rear-inflow jet, where it was also quite dry. The warm anomaly centered near 400 mb in the region of the decaying stratiform region (possessing high relative humidity) suggests a strong positive virtual potential temperature anomaly in this region, consistent with the modeling study of Zhang and Fritsch (1988a)

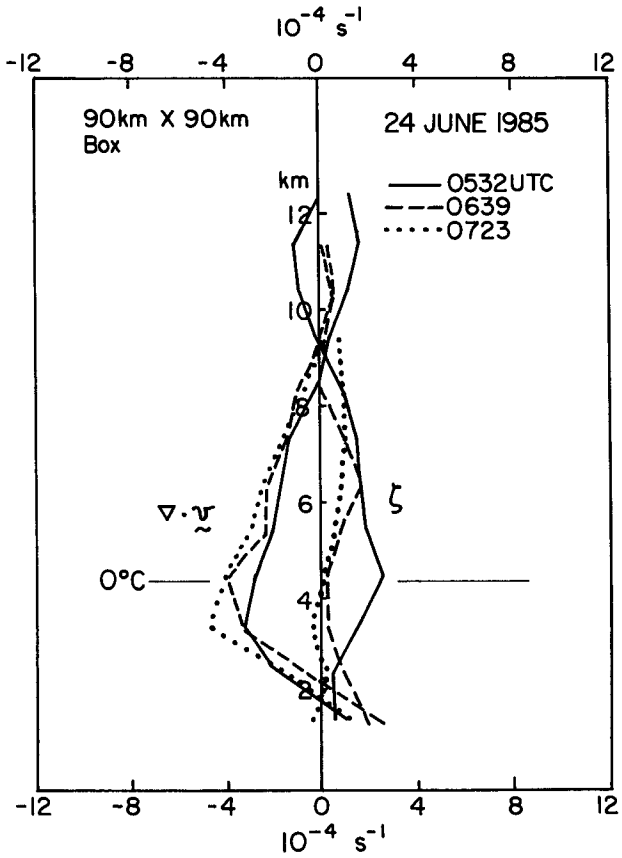


FIG. 11. As in Fig. 10, except for divergence and relative vorticity ($10^{-4}$ $s^{-1}$).

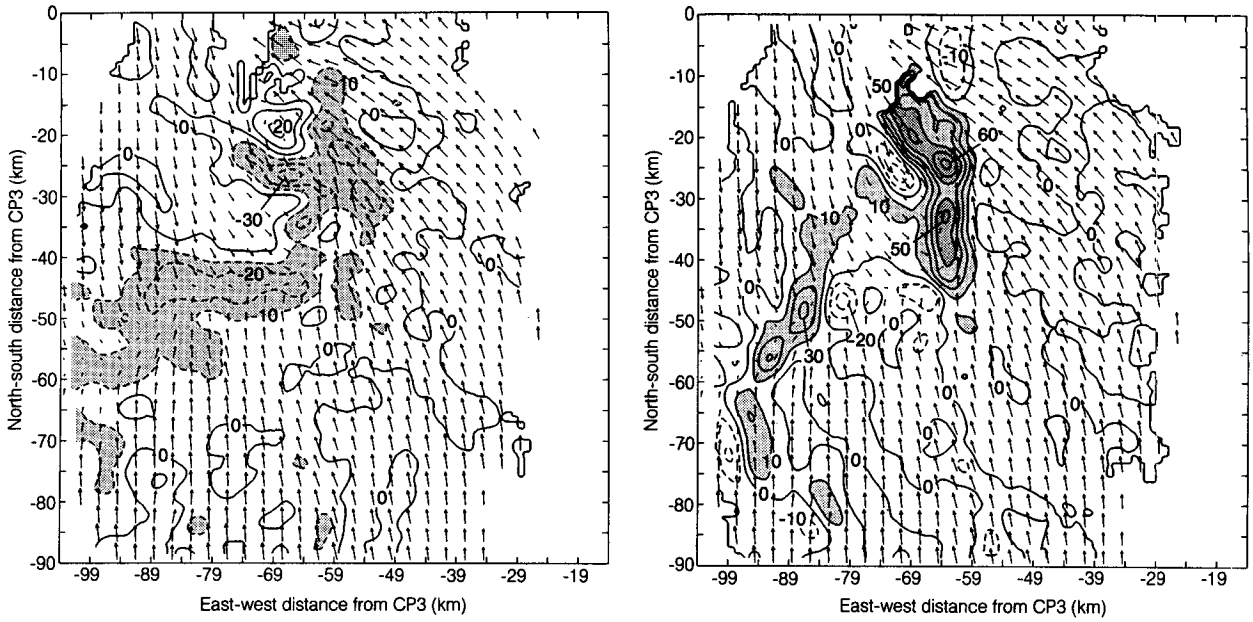


FIG. 12. System-relative winds and (a) divergence and (b) relative vorticity ($10^{-4}$ s$^{-1}$) at 0532. Values of divergence $< -10$ units and relative vorticity $> 10$ units are stippled (>40, heavy stippling).

and the mesovortex composite study of Bartels and Maddox (1991). A slight cool anomaly was actually present between 500 and 600 mb across the entire system, thus giving rise to the peculiar structure seen in Fig. 7b at 500 mb, where there was a suggestion of a cold-core structure to the mesovortex. The existence of this cool layer may have been, in part, a result of evaporation and, below the 0°C level (Fig. 14c), melting. This cold-core structure suggests that the mesovortex may have formed in the descending rear inflow, a mechanism proposed by Biggerstaff and Houze (1991) and Zhang (1992); however, data are unavailable to confirm the precise formation process in this case. Thus, although the mesovortex can be described as being warm core, this description best applies at the time of analysis to the 450–300-mb levels (Fig. 14c) rather than to the 500-mb level, where the warmest air was shifted north of the vorticity center.

## 7. Vorticity budget

In principle, a vorticity budget for the mesovortex should be possible using dual-Doppler data. However, the lack of data on the north side of the circulation complicates such an effort. Therefore, the vorticity budget has been examined using sounding data only. Unfortunately, a complete budget is not possible since adequate data only exists at a single time (0900) and storage effects cannot be computed.

It is important to emphasize that the vorticity budget computed here is relevant only to the decaying stage of the mesoscale convective system. Recent modeling studies by D.-L. Zhang (1992) indicate that there is a considerable variation in the vorticity dynamics of squall-line systems over their life cycle (at least for those occurring in environments having large along-line vertical wind shear, e.g., the 10–11 June PRE-STORM squall line). He finds that tilting and advection are important in the formative stages of the mesovortex, whereas convergence (stretching) production dominates in the decaying stage. The 23–24 June squall line studied here occurred in an environment with considerably weaker vertical wind shear (Fig. 8) than the 10–11 June squall line, suggesting a potentially weaker role of tilting in the mesovortex spinup.

Here the vorticity equation is used in the following approximate form:

$$\frac{\partial \zeta}{\partial t} \approx -u\frac{\partial \zeta}{\partial x} - v\frac{\partial \zeta}{\partial y} - \omega\frac{\partial \zeta}{\partial p} + (\zeta + f)\frac{\partial \omega}{\partial p} + \frac{\partial u}{\partial p}\frac{\partial \omega}{\partial y} - \frac{\partial v}{\partial p}\frac{\partial \omega}{\partial x}, \quad (1)$$

where $\zeta$ is the vertical component of the relative vorticity. Frictional effects (due to cumulus convection) are neglected, since by 0900 virtually all convection and precipitation had ceased (Fig. 7b). In this analysis all of the terms are computed on the rhs of (1) and the residual is attributed to storage effects. By way of contrast, vorticity-budget studies involving active cumulus convection compute a residual arising from all terms including storage (frequently referred to as $Z$; e.g., Reed and Johnson 1974; Sui and Yanai 1986) and then normally attribute the residual to convective transports.

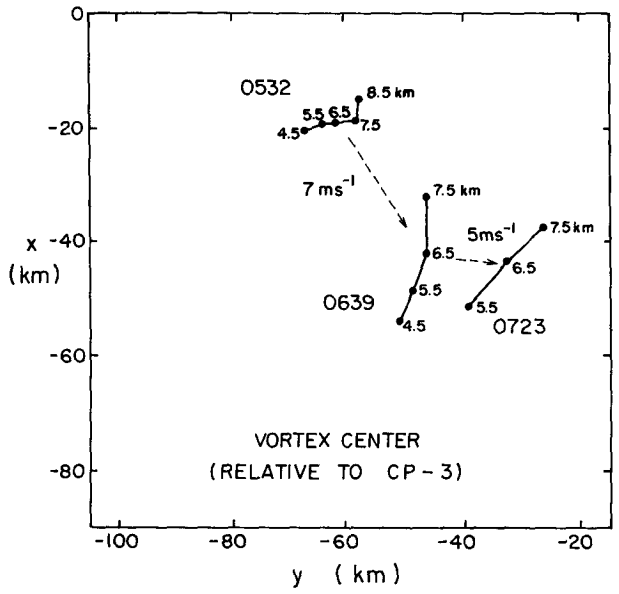


FIG. 13. Position of vortex center at various altitudes and times relative to CP-3. Speed of center at 6.5 km is indicated.

Terms in (1) have been computed for a 1° lat × 1° long area centered at the position of maximum relative vorticity at 500 mb (just northeast of WWR in Fig. 7b; see Fig. 1). Profiles of relative vorticity and vertical velocity averaged over this area are shown in Fig. 15. The profile shapes agree very well with the independently derived dual-Doppler $\zeta$ and $w$ profiles at 0639 and 0723 (Figs. 10 and 11), even though the areas are not exactly coincident and the times are not the same. Maxima in $\zeta$ and $w$ occurred near 550 mb (5 km MSL) and 650 mb (4 km), respectively. The magnitude of $\zeta$ obtained by both methods is in good agreement, while the peak in downward motion was about five times less than the Doppler-derived results. These findings indicate a persistence of the mesovortex circulation past 0723 to 0900, but a general weakening of the mesoscale downdraft as the precipitation ceased.

The terms in the vorticity budget are illustrated in Fig. 16. During the decaying stage of the storm, convergence production or stretching was the prominent mechanism for the generation of vorticity in the midtroposphere, considerably outweighing advection and tilting effects. This finding agrees with the computations of Brandes (1990) for the midlevel portion of the 7 May 1985 PRE-STORM mesovortex; however, he found important additional contributions by tilting to the low-level vorticity budget in that storm. The time tendency, calculated as a residual, indicates a continued intensification of the mesovortex at this time at a rate sufficient to double $\zeta$ at 500 mb in 2.7 h. The cessation of precipitation (and reduction in associated mesoscale updrafts and downdrafts) after 0900, however, probably significantly reduced the production rate by convergence after this time. Once produced, however, the midlevel mesovortex persisted for an extended period (Part I), as often occurs for inertially stable, warm-core mesovortices (Zhang and Fritsch 1987, 1988a,b). The Rossby radius of deformation for this case (based on an inertial–gravity-wave speed of 25 m $s^{-1}$) is approximately 300 km, a horizontal scale comparable to that of the stratiform region. The "dynamically large" scale of the stratiform region in this case is consistent with the development of a relatively long-lived, quasi-balanced mesovortex (Zhang and Fritsch 1988a; Cotton et al. 1989).

Vorticity production by tilting, which has been found to be important in mesoscale convective systems occurring in strong vertical wind shear (Verlinde and Cotton 1990; Biggerstaff and Houze 1991; Zhang 1992), is in this case less important (Fig. 16). However, this seeming distinction with other studies must be interpreted with caution since it is based on a vorticity budget that 1) uses sounding data only and 2) has been computed only for the decaying stage of the squall line. The vorticity budget results of Biggerstaff and Houze (1992), which show tilting to be important for the 10–11 June squall line, are based on a composite of sounding and radar data over the late growing, mature, and early dissipating stages of that system. As mentioned earlier, the recent modeling work of Zhang (1992) has shown stretching production to be dominant in the decaying stages (consistent with this study's results), although tilting is important earlier on. The subsequent long-lived behavior of the 23–24 June mesovortex was likely aided by the weak vertical wind shear (e.g., Velasco and Fritsch 1987; Bartels and Maddox 1991).

The strong divergence at low levels contributed to an apparent production of pronounced anticyclonic vorticity near the ground (Fig. 16). However, the development of a significant surface anticyclone appears to have been inhibited (Fig. 15) by the surface frictional torque, a term that has been omitted from (1). Its value is difficult to estimate precisely; however, if the torque is approximated by $\mathbf{k}\cdot\nabla\times(C_D|\mathbf{v}|\mathbf{v})/H$, where the drag coefficient $C_D = 0.005$ and the boundary-layer depth $H = 500$ m, then a frictional torque of $0.9 \times 10^{-4}$ $s^{-1}$ is obtained. This value compensates for nearly two-thirds of the convergence production at 900 mb.

Finally, at upper levels (200 mb) a strong cyclonic tendency is deduced, primarily as a result of advection and tilting. This behavior probably reflects the weakening of the upper-level anticyclone that was generated at an earlier time by deep cumulus convection.

## 8. Schematic of mesovortex

A schematic of the evolution of the mesovortex is presented in Fig. 17. During the squall-line decaying stage (time $t$), the storm was characterized by a leading convective line and trailing stratiform region. The rear edge of the stratiform region was deformed into a cusp

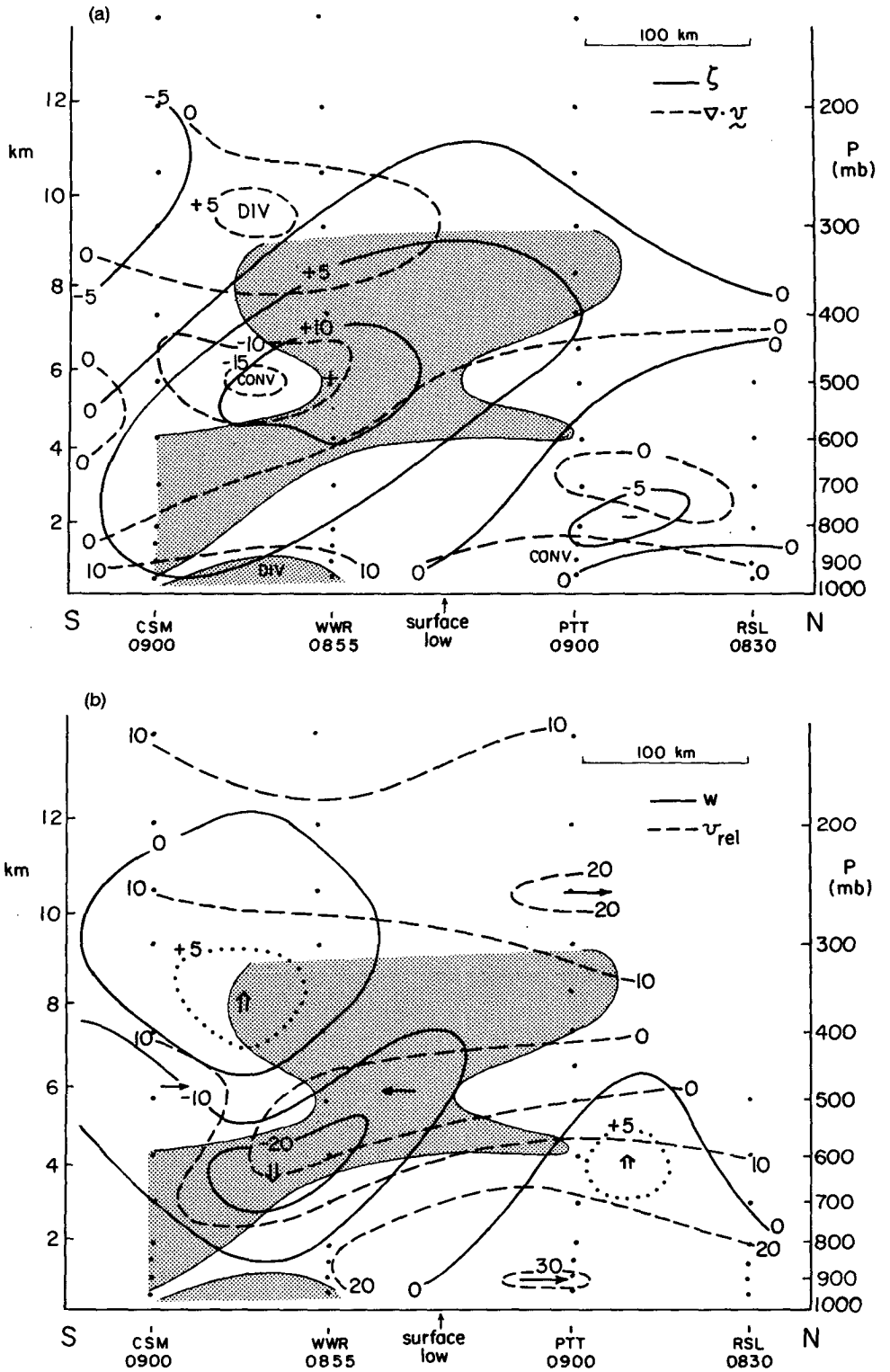


FIG. 14. North–south vertical cross section of (a) relative vorticity (solid) and divergence (dashed), both in $10^{-5}$ s$^{-1}$, (b) vertical velocity (cm s$^{-1}$, solid) and system-relative $v$ component (m s$^{-1}$, dashed), and (c) temperature anomaly (°C, solid; departure from presquall average sounding at 0515 UTC) and relative humidity (%, dashed) at 0900 UTC. Dots indicate sounding positions, whereas ×'s in (c) indicate subjectively determined sounding based on horizontal analyses at seven different pressure levels. Shading denotes RH > 80%. Heavy dotted line is 0°C isotherm.

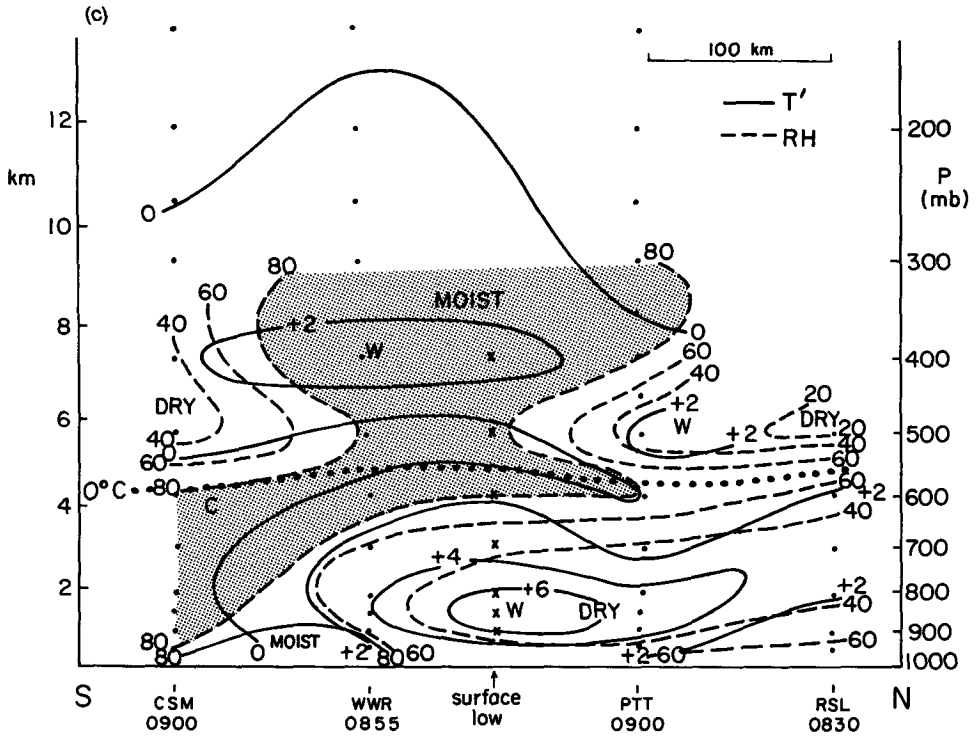


FIG. 14. (*Continued*)

or hooklike pattern by a developing cyclonic circulation embedded within a synoptic-scale short-wave trough. The formation of the mesovortex occurred outside the domain of the research radars and sounding network so that the location and timing of the initial circulation could not be determined. A vorticity budget based on the sounding data indicates that convergence production of vorticity at midlevels, associated with front-to-rear flow ahead of the system and the rear-inflow jet behind, appears to have contributed to an intensification of the mesovortex during the decaying stage of the precipitation system. The mesovortex was confined to the midtroposphere between 3 and 8 km, and its axis tilted toward the northeast.

Four hours later (Fig. 17), the storm completely dissipated and precipitation ceased, but the cyclonic circulation at 500 mb persisted and expanded. In addition, a pronounced surface low developed beneath the mesovortex (also shown in Fig. 12d of Part I). The mesovortex continued for at least 3–6 h longer near the Kansas–Oklahoma border and was associated with the later development of convective precipitation over southwestern Kansas.

## 9. Summary and conclusions

Surface, sounding, and dual-Doppler radar data from OK PRE-STORM have been used to document the

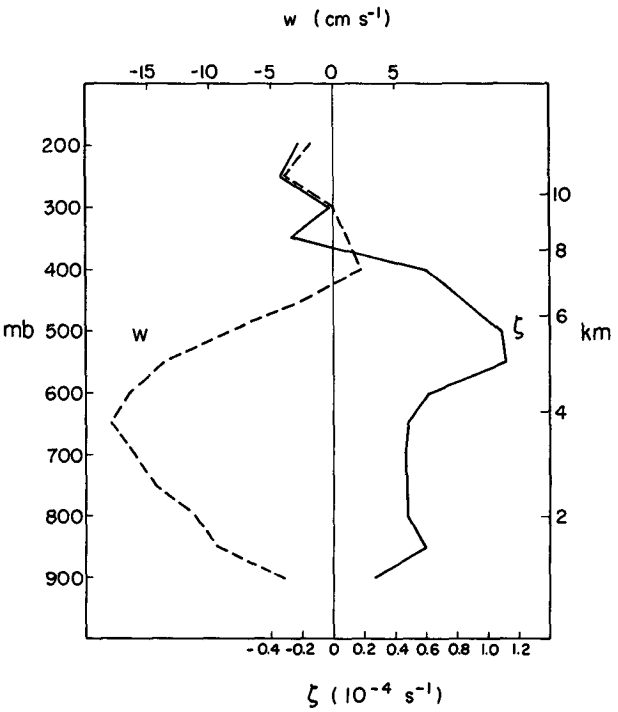


FIG. 15. Relative vorticity ($10^{-4}$ s$^{-1}$) and vertical velocity (cm s$^{-1}$) averaged over a 1° lat × 1° long area centered on the mesovortex at 0900 UTC.

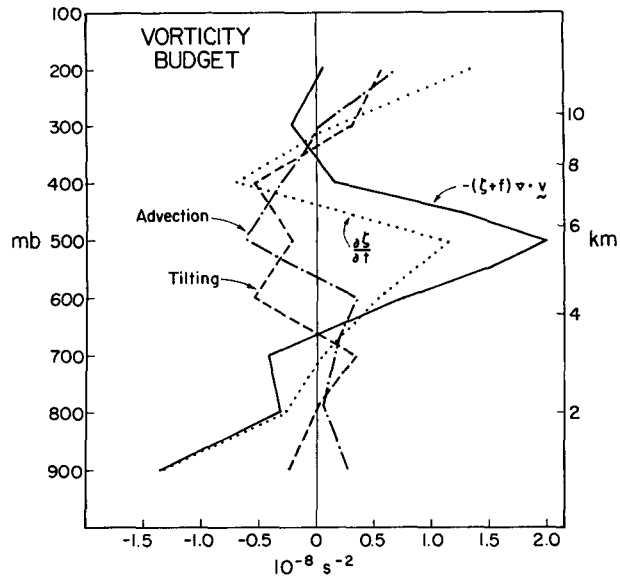


FIG. 16. Terms in vorticity budget ($10^{-8}$ s$^{-2}$) over 1° lat × 1° long area centered on the mesovortex at 0900 UTC.

structure of a midlevel mesovortex that developed within the trailing stratiform precipitation region of a decaying mesoscale convective system on 23–24 June 1985. Although the formation of the mesovortex occurred outside the PRE-STORM mesonetwork, data obtained when the circulation was within it indicate that the system was closely coupled with a synoptic-scale short-wave trough passing across the central United States. A closed circulation developed coincident with the trough axis and at the back edge of the trailing stratiform precipitation region. The vortex, which had a horizontal dimension of ~100 km, deformed the stratiform region into a hooklike pattern. It was confined to the midtroposphere (3–8 km) and tilted northeastward with height. The temperature structure was complex and apparently strongly influenced by a rapidly descending rear-inflow jet at the rear edge of the stratiform region. Near the circulation center, a pronounced warm anomaly existed at low levels (near 850 mb), with a cool anomaly at midlevels near the 0°C level and a weak warm anomaly aloft. The vertical structure of the 23–24 June 1985 mesovortex bore a close resemblance to the simulation of a 7–8 July 1982 case by Zhang and Fritsch (1988b). It also supports the general findings of Bartels and Maddox (1991) regarding the kinematic and thermodynamic structure of their composite mesovortex based on conventional sounding data.

Analyses of the vorticity budget from sounding data strongly indicate convergence production or vortex stretching to be a prominent mechanism in the inten-

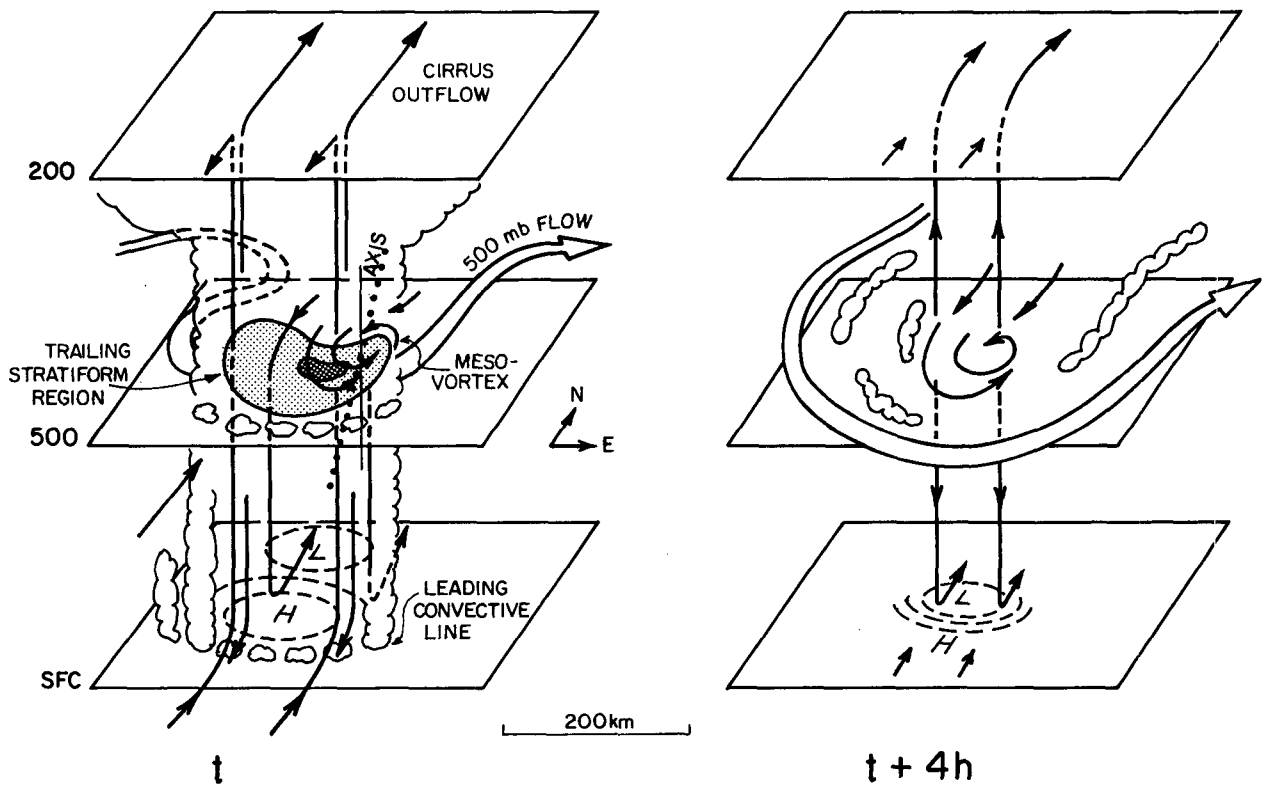


FIG. 17. Idealized cloud and system-relative flow structure during decaying squall-line stage ($t$) and fully developed mesovortex stage ($t$ + 4 h). Solid arrows denote storm-relative flow, and open arrows large-scale 500-mb flow. Dotted line indicates approximate vertical extent and tilt (toward the northeast) of mesovortex core.

sification of the mesovortex during the decaying stage of the squall line. This midtropospheric convergence was a consequence of the mesoscale updraft–downdraft couplet associated with the stratiform region of the dissipating mesoscale convective system. Although tilting has been diagnosed to play an important role in the vorticity budget of squall-line systems in strongly sheared environments (Verlinde and Cotton 1990; Biggerstaff and Houze 1991; Zhang 1992), the weakly sheared environment of the 23–24 June mesovortex appears to have minimized tilting effects. However, this conclusion must be considered tentative when applied to the entire life cycle of the mesovortex since data were not available for a vorticity budget during its formative stage.

The mesovortex development in this case was associated with a preexisting short-wave trough. This feature has been incorporated into the schematic in Fig. 17. Evidence also exists from other studies (Leary and Rappaport 1987; Zhang and Fritsch 1987, 1988a,b; Brandes 1990; Bartels and Maddox 1991) of a possible role of a short-wave trough in mesovortex development. Such troughs may play an instrumental role in the vortex spinup by providing positive ambient relative vorticity. In addition, Zhang and Gao (1989) have argued that baroclinity associated with short-wave troughs can make an important contribution to the rear-inflow jet, in addition to in situ generation due to processes within the squall line itself (Smull and Houze 1987; Lafore and Moncrieff 1989). Typically, rear-to-front jets are found initially at upper levels, and their descent to midlevels is accomplished through precipitation sublimation or evaporation, or both, aloft in the stratiform region (Zhang and Gao 1989; Stensrud et al. 1991). These jets, in turn, may play an important role in the vortex spinup by enhancing midlevel convergence.

However, the extent to which short-wave troughs are a prerequisite for mesovortex formation is not well known. Mesoscale convective systems (having attendant stratiform precipitation regions) that form apart from any short-wave trough activity should, in principle, still be able to develop a mesovortex as a result of convergence of planetary vorticity alone. However, documentation of such events is limited.

While some portion of the lifetime of the 23–24 June 1985 mesovortex was sampled by dual-Doppler radars, the motion of the system restricted the period of analysis for this case to just a few hours. The planned installation of the National Weather Service wind-profiling and Doppler radar networks should significantly enhance the opportunities for capturing the gross kinematic features of mesovortex phenomena.

*Acknowledgments.* The assistance of Sue Chen and Greg Stumpf in the early stages of the analysis is appreciated. Brad Smull provided valuable guidance with the dual-Doppler analyses. Comments on the manuscript by Da-Lin Zhang, Bill Gallus, and an anonymous reviewer have been very helpful, as have been discussions on this subject with Da-Lin Zhang and Wayne Schubert. This research has been supported by the National Science Foundation, Atmospheric Sciences Division, under Grants ATM-8711649 and ATM-9013112, and National Atmospheric and Oceanic Administration Grant NA90RAH00077.

## REFERENCES

Bartels, D. L., 1989: Mid-level cyclonic vortices generated by mesoscale convective systems. M.S. thesis, Department of Meteorology, University of Oklahoma, Norman, 131 pp. [Available from the author at NSSL MRD, R/E/NS1, 325 Broadway, Boulder, CO 80303.]

——, and R. A. Maddox, 1991: Midlevel cyclonic vortices generated by mesoscale convective systems. *Mon. Wea. Rev.*, **119**, 104–118.

Biggerstaff, M. I., and R. A. Houze, Jr., 1991: Midlevel vorticity structure of the 10–11 June 1985 squall line. *Mon. Wea. Rev.*, **119**, 3066–3079.

Brandes, Edward A., 1990: Evolution and structure of the 6–7 May 1985 mesoscale convective system and associated vortex. *Mon. Wea. Rev.*, **118**, 109–127.

Brown, J. M., 1979: Mesoscale unsaturated downdrafts driven by rainfall evaporation: A numerical study. *J. Atmos. Sci.*, **36**, 313–338.

Cotton, W. R., M.-S. Lin, R. L. McAnelly, and C. J. Tremback, 1989: A composite model of mesoscale convective complexes. *Mon. Wea. Rev.*, **117**, 765–783.

Crook, N. A., R. E. Carbone, M. W. Moncrieff, and J. W. Conway, 1990: The generation and propagation of a nocturnal squall line. Part II: Numerical simulations. *Mon. Wea. Rev.*, **118**, 50–65.

Fritsch, J. M., and C. G. Chappell, 1980: Numerical prediction of convectively driven mesoscale pressure systems. Part II: Mesoscale model. *J. Atmos. Sci.*, **37**, 1734–1762.

Fujita, T. T., 1955: Results of detailed synoptic studies of squall lines. *Tellus*, **7**, 405–436.

Gamache, J. F., and R. A. Houze, Jr., 1982: Mesoscale air motions associated with a tropical squall line. *Mon. Wea. Rev.*, **10**, 118–135.

Hertenstein, R. F. A., and W. H. Schubert, 1991: Potential vorticity anomalies associated with squall lines. *Mon. Wea. Rev.*, **119**, 1663–1672.

Houze, R. A., Jr., 1977: Structure and dynamics of a tropical squall-line system. *Mon. Wea. Rev.*, **105**, 1540–1567.

——, and E. N. Rappaport, 1984: Air motions and precipitation structure of an early summer squall line over the eastern tropical Atlantic. *J. Atmos. Sci.*, **41**, 553–574.

——, S. A. Rutledge, M. I. Biggerstaff, and B. F. Smull, 1989: Interpretation of Doppler weather radar displays of midlatitude mesoscale convective systems. *Bull. Amer. Meteor. Soc.*, **70**, 608–619.

——, B. F. Smull, and P. Dodge, 1990: Mesoscale organization of springtime rainstorms in Oklahoma. *Mon. Wea. Rev.*, **118**, 613–654.

——, S. A. Rutledge, M. I. Biggerstaff, and B. F. Smull, 1989: Interpretation of Doppler weather radar displays of midlatitude mesoscale convective systems. *Bull. Amer. Meteor. Soc.*, **70**, 608–619.

Hoxit, L. R., C. F. Chappell, and J. M. Fritsch, 1976: Formation of mesolows or pressure troughs in advance of cumulonimbus clouds. *Mon. Wea. Rev.*, **104**, 1419–1428.

Johnson, B. C., 1983: The heat burst of 29 May 1976. *Mon. Wea. Rev.*, **111**, 1776–1792.

Johnson, R. H., and P. J. Hamilton, 1988: The relationship of surface pressure features to the precipitation and air flow structure of an intense midlatitude squall line. *Mon. Wea. Rev.*, **116**, 1444–1472.

——, S. Chen, and J. J. Toth, 1989: Circulations associated with a mature-to-decaying midlatitude mesoscale convective system. Part I: Surface features—Heat bursts and mesolow development. *Mon. Wea. Rev.*, **117,** 942–959.

Johnston, E. C., 1982: Mesoscale vorticity centers induced by mesoscale convective complexes. Preprints, *Ninth Conf. on Weather Forecasting and Analysis,* Seattle, Amer. Meteor. Soc., 196–200.

Kuo, Y.-H., L. Cheng, and R. A. Anthes, 1986: Mesoscale analysis of the Sichuan flood catastrophe, 11–15 July 1981. *Mon. Wea. Rev.*, **114,** 1984–2003.

Lafore, J.-P., and M. W. Moncrieff, 1989: A numerical investigation of the organization and interaction of the convective and stratiform regions of tropical squall lines. *J. Atmos. Sci.*, **46,** 521–544.

Leary, C. A., 1979: Behavior of the wind field in the vicinity of a cloud cluster in the intertropical convergence zone. *J. Atmos. Sci.*, **36,** 631–639.

——, and R. A. Houze, Jr., 1979: Melting and evaporation of hydrometeors in precipitation from the anvil clouds of deep tropical convection. *J. Atmos. Sci.*, **36,** 669–679.

——, and E. N. Rappaport, 1987: The life cycle and internal structure of a mesoscale convective complex. *Mon. Wea. Rev.*, **115,** 1503–1527.

Menard, R. D., and J. M. Fritsch, 1989: An MCC-generated inertially stable warm core vortex. *Mon. Wea. Rev.*, **117,** 1237–1261.

Ogura, Y., and M. T. Liou, 1980: The structure of a mid-latitude squall line. A case study. *J. Atmos. Sci.*, **37,** 553–567.

Ray, P. S., C. L. Ziegler, W. Bumgarner, and R. J. Serafin, 1980: Single- and multiple-Doppler radar observations of tornadic storms. *Mon. Wea. Rev.*, **108,** 1607–1625.

Raymond, D. J., and H. Jiang, 1990: A theory for long-lived mesoscale convective systems. *J. Atmos. Sci.*, **47,** 3067–3077.

Reed, R. J., and R. H. Johnson, 1974: The vorticity budget of synoptic-scale wave disturbances in the tropical western Pacific. *J. Atmos. Sci.*, **31,** 1784–1790.

Roux, F., J. Testud, M. Payen, and B. Pinty, 1984: West African squall-line thermodynamic structure retrieved form dual-Doppler radar observations. *J. Atmos. Sci.*, **11,** 3104–3121.

Rutledge, S. A., R. A. Houze, Jr., M. I. Biggerstaff, and T. Matejka, 1988: The Oklahoma–Kansas mesoscale convective system of 10–11 June 1985: Precipitation structure and single-Doppler radar analysis. *Mon. Wea. Rev.*, **116,** 1409–1430.

Schubert, W. H., J. J. Hack, P. L. Silva Dias, and S. R. Fulton, 1980: Geostrophic adjustment in an axisymmetric vortex. *J. Atmos. Sci.*, **37,** 1464–1484.

Smull, B. F., and R. A. Houze, Jr., 1985: A midlatitude squall line with a trailing region of stratiform rain: Radar and satellite observations. *Mon. Wea. Rev.*, **113,** 117–133.

——, and ——, 1987: Rear inflow in squall lines with trailing stratiform precipitation. *Mon. Wea. Rev.*, **115,** 2869–2889.

Smull, B. F., D. P. Jorgensen, and C. E. Hane, 1991: Comparison of retrieved pressure and buoyancy perturbations with in situ observations of an intense wake low in a midlatitude mesoscale convective system. Preprints, *25th Int. Conf. on Radar Meteorology,* Paris, Amer. Meteor. Soc., 135–138.

Stensrud, D. J., and R. A. Maddox, 1988: Opposing mesoscale circulations: A case study. *Wea. Forecasting,* **3,** 189–204.

——, ——, and C. L. Ziegler, 1991: A sublimation-initiated mesoscale downdraft and its relation to the wind field below a precipitating anvil cloud. *Mon. Wea. Rev.*, **119,** 2124–2139.

Stirling, J., and R. M. Wakimoto, 1989: Mesoscale vorticies in the stratiform region of a decaying midlatitude squall line. *Mon. Wea. Rev.*, **117,** 452–458.

Stumpf, G. J., R. H. Johnson, and B. F. Smull, 1991: The wake low in a midlatitude mesoscale convective system having complex organization. *Mon. Wea. Rev.*, **119,** 134–158.

Sui, C.-H., and M. Yanai, 1986: Cumulus ensemble effects on the large-scale vorticity and momentum fields of GATE. Part I: Observational evidence. *J. Atmos. Sci.*, **43,** 1618–1642.

Velasco, I., and J. M. Fritsch, 1987: Mesoscale convective complexes in the Americas. *J. Geophys. Res.*, **92,** 9591–9613.

Verlinde, J., and W. R. Cotton, 1990: Mesoscale vortex-couplet observed in the trailing anvil of a multicellular convective complex. *Mon. Wea. Rev.*, **118,** 993–1010.

Welander, P., 1955: Studies on the general development of motion in a two-dimensional ideal fluid. *Tellus,* **7,** 141–156.

Wetzel, P. J., W. R. Cotton, and R. L. McAnelly, 1983: A long-lived mesoscale convective complex. Part II. Evolution and structure of the mature complex. *Mon. Wea. Rev.*, **111,** 1919–1937.

Zhang, D.-L., 1992: Formation of a cooling-induced mesovortex in the trailing stratiform region of a midlatitude squall line. *Mon. Wea. Rev.*, (in press).

——, D.-L., and J. M. Fritsch, 1987: Numerical simulation of the mesobeta-scale structure and evolution of the 1977 Johnstown flood. Part II: Inertially stable warm-core vortex and the mesoscale convective complex. *J. Atmos. Sci.*, **44,** 2593–2612.

——, and ——, 1988a: Numerical sensitivity experiments of varying model physics on the structure, evolution and dynamics of two mesoscale convective systems. *J. Atmos. Sci.*, **45,** 261–293.

——, and ——, 1988b: A numerical investigation of a convectively generated, inertially stable, extratropical warm-core mesovortex over land. Part I: Structure and evolution. *Mon. Wea. Rev.*, **116,** 2660–2687.

——, and K. Gao, 1989: Numerical simulation of an intense squall line during 10–11 June 1985 PRE-STORM. Part II: Rear inflow, surface pressure perturbations, and stratiform precipitation. *Mon. Wea. Rev.*, **117,** 2067–2094.

Zipser, E. J., 1977: Mesoscale and convective-scale downdrafts as distinct components of squall-line circulation. *Mon. Wea. Rev.*, **105,** 1568–1589.